Journal of King Saud University - Science 36 (2024) 103530

HOSTED BY

Contents lists available at ScienceDirect

Journal of King Saud University - Science

journal homepage: www.sciencedirect.com

# Effect of heat generation on MHD Maxwell fluid flow on a stretching cylinder embedded in a porous medium along with impact of radiation

Umadevi Raj [a], Prabhakar Sagadevan [b], Nazek Alessa [c,*]

[a] Department of Mathematics, Sri Venkateswara College of Engineering, Irrungattukottai, Tamil Nadu, India
[b] Department of Mathematics, S. A. Engineering College, Chennai, Tamilnadu, India
[c] Department of Mathematical Sciences, College of Science, Princess Nourah bint Abdulrahman University, P.O. Box 84428, Riyadh 11671, Saudi Arabia

ARTICLE INFO

*Keywords:*
MHD
Maxwell fluid
Radiation
Stretching cylinder
Porous medium
Heat generation

ABSTRACT

This study addresses the critical problem of understanding Maxwell fluids' thermal and flow behavior in the occurrence of magnetohydrodynamics (MHD), radiation, and heat generation over a stretching cylinder, which is of significant importance in various industrial applications such as polymer processing and heat exchangers. The novelty of this work lies in its detailed exploration of the curvature parameter ($\alpha_e$) and its influence on the flow dynamics, extending beyond the scope of previous literature. The governing equations, incorporating the impacts of MHD, radiation, and heat generation, are derived and subsequently simplified using similarity transformations to convert them into ordinary differential equations. These equations are then solved numerically via the bvp4c solver in MATLAB. The results are presented through tables and graphical representations to deliver clear insights into the behavior of key non-dimensional parameters. Quantitative findings reveal that the temperature profile of the fluid increases with higher heat generation and radiation, with specific enhancements observed on both flat plates (curvature parameter $\alpha_e = 0$) and cylindrical surfaces ($\alpha_e = 1$). Our results are consistent with existing studies, validating the robustness of our numerical approach.

## 1. Introduction

Studying fluid dynamics in the presence of complex physical phenomena is crucial for advancing various engineering applications. In this context, the flow of Maxwell fluid over a cylinder provides significant perceptions into the behavior of viscoelastic fluids under different conditions. This manuscript explores the intricate interplay of several factors, including radiation heat generation, magnetohydrodynamics (MHD), and porous media, in the flow dynamics of Maxwell fluids. Radiation heat generation contributes to the thermal field, influencing the fluid's temperature distribution and overall heat transfer characteristics. Concurrently, MHD effects, driven by the interaction of the fluid with an external magnetic field, introduce additional complexities in the fluid's behavior, impacting both the velocity and temperature fields. The inclusion of a porous medium further adds to the complexity by altering the flow resistance and heat transfer characteristics.

In the field of fluid dynamics and heat transfer, extensive research has been conducted to understand the behavior of Maxwell and hybrid nanofluids under various conditions. Maxwell's foundational work in (1881) introduced a rate-type model that effectively predicts viscoelastic and stress-relaxation behaviors in materials, laying the groundwork for subsequent studies. Crane's (1975) exploration of boundary layer flow near stretched cylinders and Grubka and Bobba's (1985) investigation into energy transfer on stretching surfaces with variable temperatures further contributed to the understanding of fluid–solid interactions and heat exchange dynamics. Building on this, Wang's (1988) study on viscous liquid flow around extended hollow cylinders and Reddy Gorla and Sidawi's (1994) research on natural convection on vertical stretching surfaces expanded the knowledge of boundary layer flows and slip effects. Ishak's (2010) work on energy boundary layer flow in micropolar fluids and Mukhopadhyay's (2012) exploration of heat transfer in time-dependent Maxwell fluid flows introduced the significant effects of radiation and heat sources in fluid dynamics.

The early 2010 s saw a surge in research focusing on more complex fluid systems. Yang et al. (2013) delved into the energy conductivity of Maxwell fluids in two-phase media, while Ramzan et al. (2016) and Markin et al. (2017) explored convective flows and stagnation point heat transfer, respectively. Irfan et al. (2018) advanced the field by employing the Homotopy Analysis Method to solve flow problems involving Maxwell fluids with heat sinks. In 2019, Ahmed et al.

* Corresponding author.
*E-mail address:* naalessa@pnu.edu.sa (N. Alessa).

https://doi.org/10.1016/j.jksus.2024.103530
Received 1 July 2024; Received in revised form 28 September 2024; Accepted 6 November 2024
Available online 22 November 2024

**Nomenclature**

Ambient fluid Concentration $C_\infty$
Ambient fluid temperature $T_\infty$
Concentration of the fluid $C$
Concentration on the wall $C_w$
Curvature parameter $\alpha_e$
Deborah number $\beta_p$
Density of the fluid ρ
Dimensional Porosity parameter $K$
Dimensional heat generation $Q_b$
Dimensionless concentration $\phi$
Dimensionless heat generation $Q_p$
Dimensionless radiation $R_P$
Dimensionless stream function s
Directions $z$, $r$
Electrical Conductivity $\sigma$
Kinematic Viscosity γ
Local Nusselt number $Nu_x$
Local Reynolds number $Re_x$
MHD parameter $M_p$
Mass diffusion $D_B$
Maxwell fluid parameter $\lambda_4$
Mean absorption coefficient $k^*$
non-dimensional temperature $\theta$
Prandtl number $Pr$
Reference length $L$
Schmidt number $Sc$
Sherwood number $Sh_x$
Similarity variable $\eta_1$
Skin friction coefficient $C_f$
Specific heat $C_p$
Stefan blowing parameter $Sb_m$
Stefan-Boltzmann constant $\sigma^*$
Strength of magnetic field $B_0$
Surface heat flux $q_w$
Temperature of the fluid $T$
Temperature on the wall $T_w$
Thermal conductivity $k$
Thermal diffusivity $\alpha$
Thermal viscosity $\mu$
Velocities of the fluid $u^*$, $v^*$

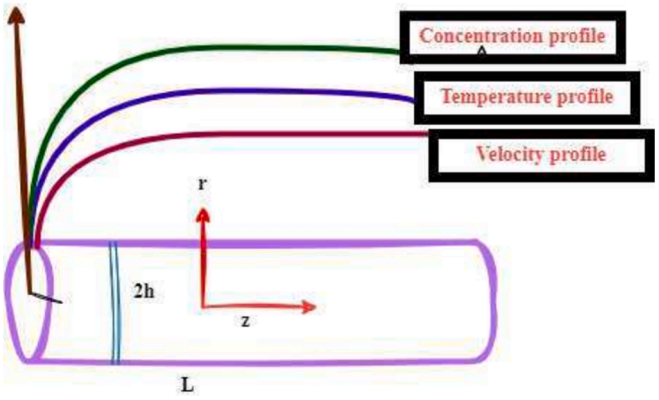


**Fig. 1.** Schematic diagram for horizontal diagram

examined heterogeneous-homogeneous reactions and non-Fourier heat flux theory in Oldroyd-B fluids, highlighting the profound influence of chemical reactions on complex fluid systems.

The 2020 s introduced new dimensions to the investigation of Maxwell and hybrid nanofluids, particularly in the context of magnetohydrodynamics. Ahmed et al. (2020) investigated the MHD flow of Maxwell nanofluids, exploring radiation and convective energy transport, while Zhao (2020) focused on axisymmetric convection flow in geometrically complex scenarios. Loganathan et al. (2021) incorporated the Cattaneo-Christov model into the study of Maxwell fluids, furthering the understanding of multi-physical interactions in fluid systems. Khan et al. (2021) and Sajid et al. (2022) explored the Cattaneo-Christov theory's application to Maxwell fluid flow. Recent advances by Biswas et al. (2022, 2024) and Mandal et al. (2022, 2023) have highlighted the significant role of magnetic fields and enclosure geometries in influencing thermal performance and system irreversibility in hybrid nanofluidic systems. Manna et al. (2024) conducted a constraint-based investigation of energy transport and irreversibility in magnetic thermal systems.

### *1.1. Specific contributions and advancements and potential practical applications and industrial relevance*

The practical implications of these findings are significant, particularly in industries where non-Newtonian fluids are used and precise thermal control is critical. For instance, in polymer processing, understanding the effects of radiation and heat generation on Maxwell fluid behavior can enhance control over extrusion processes, improving product quality and reducing energy consumption. Moreover, the insights from this research can inform the design of more efficient heat exchangers and cooling systems that use non-Newtonian fluids, contributing to better performance and energy efficiency in various industrial applications. These contributions not only advance academic understanding but also have direct implications for improving industrial processes, demonstrating the practical significance of the study.

### *1.2. Novelty of this study*

The extensive body of literature on Maxwell fluid dynamics has provided significant insights into boundary layer flows, energy transfer on stretching surfaces, and the effects of radiation and magnetohydrodynamics (MHD) across various geometries; however, a critical research gap remains unaddressed: none of the existing studies have investigated the collective effects of MHD, radiation, porosity, and heat generation on the flow of Maxwell fluids around cylindrical geometries. This research aims to fill that gap by thoroughly investigating these combined possessions on Maxwell fluid flow over a permeable stretching cylinder. A comprehensive comparison with existing literature validates the accuracy of our findings and highlights the consistency of our methodology. Furthermore, our study examines the effects of these parameters on both flat plates and cylindrical geometries, offering a holistic perspective on how they shape flow dynamics in different contexts.

## 2. Mathematical modelling

Consider a 2D steady flow of the MHD Maxwell fluid across a stretching cylinder of diameter '2$h$' implanted in a permeable medium. The MHD is useful perpendicular to the cylinder axis. The cylinder has the velocity $u_d z/L$ along the $z$ direction; here, $u_d$ means the velocity, and $L$ means the specific length. Energy and concentration of the Maxwell fluid are constant at the cylinder's surface $T = T_\infty$ and $C = C_\infty$. Let $(z, r)$

**Table 1**
Comparing the skin friction coefficient across various studies using different values for $M_p$ while $\alpha_e = 0 = \beta_p$.

| $M_p$ | Ahmed et al. [1] | Ahmed et al. [2] | Outcomes of this study |
|---|---|---|---|
| 0.5 | 1.224745 | 1.224742 | 1.224745 |
| 1.0 | 1.414213 | 1.414213 | 1.414214 |
| 1.5 | −— | 1.581136 | 1.581139 |
| 2.0 | −— | 1.732045 | 1.732051 |
| 5.0 | 2.449474 | 2.446251 | 2.449490 |

**Table 2**
Comparison of Nusselt number for various Pr values.

| Pr | RK45Ref [24] | The outcome of this work |
|---|---|---|
| 0.72 | 0.463145 | 0.463144 |
| 1 | 0.581978 | 0.581977 |
| 3 | 1.165253 | 1.165252 |
| 10 | 2.308025 | 2.308024 |
| 100 | 7.765899 | 7.765900 |

**Table 3**
Results of $C_f$, $Nu_x$, $Sh_x$ for various values of parameters.

| $M_p$ | $\alpha_e$ | $Sb_p$ | $\beta_p$ $\phi_p$ | $R_p$ | $f''(0)$ | $Nu_x Re_x^{-1/2}$ | $Sh_x Re_x^{-1/2}$ |
|---|---|---|---|---|---|---|---|
| 0 | | | | | 1.70000 | 1.100396 | 1.002545 |
| 0.5 | | | | | 1.851437 | 1.048885 | 0.985034 |
| 2 | | | | | 2.242775 | 0.920616 | 0.945668 |
| 4 | | | | | 2.673555 | 0.793845 | 0.910683 |
| | 0 | | | | 1.804788 | 0.943040 | 0.949326 |
| | 0.3 | | | | 1.941746 | 0.599271 | 1.056166 |
| | 0.5 | | | | 2.028778 | 0.468244 | 1.126356 |
| | 1 | | | | 2.235357 | 0.365284 | 1.297585 |
| | | 0 | | | 1.862967 | 0.977521 | 1.045743 |
| | | 0.5 | | | 1.821397 | 0.337413 | 0.809416 |
| | | 1 | | | 1.801882 | 0.206791 | 0.673391 |
| | | 2 | | | 1.785161 | 0.764412 | 0.518718 |
| | | | 0 | | 1.827097 | 0.842770 | 0.989704 |
| | | | 0.2 | | 1.851434 | 0.821432 | 0.985035 |
| | | | 0.3 | | 1.863505 | 0.810711 | 0.982755 |
| | | | 0.4 | | 1.875506 | 0.799956 | 0.980512 |
| | | | | 0 | 1.851434 | 0.352602 | 0.985035 |
| | | | | 0.5 | 1.851434 | 0.618035 | 0.985035 |
| | | | | 1 | 1.851434 | 0.821432 | 0.985035 |
| | | | | 2 | 1.851435 | 1.069522 | 0.985035 |

be cylindrical polar coordinates. So that the axis is parallel to the cylinder's axis and the *r*-axis is constrained along the radial direction. Viscous dissipation is neglected because, in typical engineering scenarios with moderate velocities and common fluids like air or water, the heat generated by viscous forces is minimal compared to conduction and convection. These assumptions simplify the governing equations while still accurately representing the essential physics of the system. From Irfan et al. [9], Fig 1.

### 2.1. Continuity equation in dimensional form

$$(ru^*)_r + (rv^*)_z = 0 \tag{1}$$

### 2.2. Momentum equation in dimensional form

$$u^* v_r^* + v^* v_z^* + \lambda_4 \left[ v^{*2} v_{zz}^* + u^{*2} v_{rr}^* + 2v^* u^* v_{zr}^* \right] = v \left[ v_{rr}^* + \frac{v_r}{r} \right] - \frac{\sigma B_o^2}{\rho} \left[ \lambda_4 u^* v_r^* + v^* \right] - \frac{v v^*}{K} \tag{2}$$

### 2.3. Energy equation in dimensional form

$$u^* T_r + v^* T_z = \alpha_e \left[ T_{rr} + \frac{T_r}{r} \right] + \frac{16\sigma^* T_\infty^3 T_{rr}}{3(\rho c p) k^*} + Q_b (T - T_\infty) \tag{3}$$

## 3. 2.4 concentration equation in dimensional form

$$u^* C_r + v^* C_z = D_B \left[ C_{rr} + \frac{C_r}{r} \right] \tag{4}$$

### 3.1. Boundary conditions with the effect of Stefan parameter

$$u^* = u_w^*, v^* = \frac{-D_B C_r}{1 - C_w}, \; T = T_w, \; C = C_w \; at \;\; r = h \tag{5}$$

$$u^* \to 0, \; T \to T_\infty, \; C \to C_\infty, \; at \; r \to \infty \tag{6}$$

### 3.2. Similarity variables and non-dimensional quantities

$\phi(\eta_1) = \frac{C - C_\infty}{C_w - C_\infty}$ represents the dimensionless concentration, this parameter normalizes the concentration profile, making it independent of the specific concentrations involved. $v^* = \frac{z u_d^*}{L} s'(\eta_1), u^* = -\frac{h}{r} \sqrt{\frac{\nu u_d^*}{L}} s(\eta_1)$

The specific forms of $u^*$ and $v^*$ in your equations are tied to the similarity solutions used to reduce the complexity of the problem.

$\theta(\eta_1) = \frac{T - T_\infty}{T_w - T_\infty}$ denotes the temperature, where is the temperature at a point, $T_\infty$ means the ambient temperature, and $T_w$ is the temperature at the boundary.

$\eta_1 = \sqrt{\frac{u_d^*}{L\nu}} \left( \frac{r^2 - h^2}{2h} \right)$ is a similarity variable that combines spatial coordinates and flow properties, simplifying the governing equations by reducing the number of independent variables.

$Pr = \frac{\upsilon}{\alpha}$ indicates the relative thickness of the velocity boundary layer to the thermal boundary layer.

$\alpha = \left( \frac{L\nu}{u_d h^2} \right)^{\frac{1}{2}}$ represent a ratio involving characteristic lengths, velocities, and fluid properties, typically seen in scaling analyses.

$M_p = \frac{\sigma B_0^2 L}{\rho u_d^*}$ signifies the ratio of magnetic force to inertial force in magnetohydrodynamic (MHD) flows.

$\phi_p = \frac{\nu L}{K u_d^*}$ represents the influence of a permeable medium on the flow, where $K$ denotes the permeability of the medium.

$\beta_p = \frac{\lambda_4 u_d^*}{L}$ represents the Maxwell fluid, which personifies the viscoelastic behavior of the fluid.

$Sb_m = \frac{C_w - C_\infty}{1 - C_w}$ relates to phase change processes, such as melting or solidification, where the concentration gradient drives the phase change.

$Sc = \frac{\nu}{D_B}$ is the ratio of momentum diffusivity (kinematic viscosity $\nu$) to mass diffusivity ($D_B$).

$R_p = \frac{16\sigma^* T_\infty^3}{3kk^*}$ is radiation parameter quantifies the relative contribution of radiation to the overall heat transfer process.

### 3.3. Dimensionless momentum equation

From (2) to (6), take the following form.

$$(1 + 2\eta_1 \alpha) s''' + 2\alpha s'' - s'^2 + s s'' + 2\beta_p s s' s'' - \beta_p s^2 s''' - \frac{\alpha \beta_p}{(1 + 2\eta_1 \alpha)} s^2 s'' - M_p [s' - \beta_p s s''] - \phi_p s' = 0 \tag{7}$$

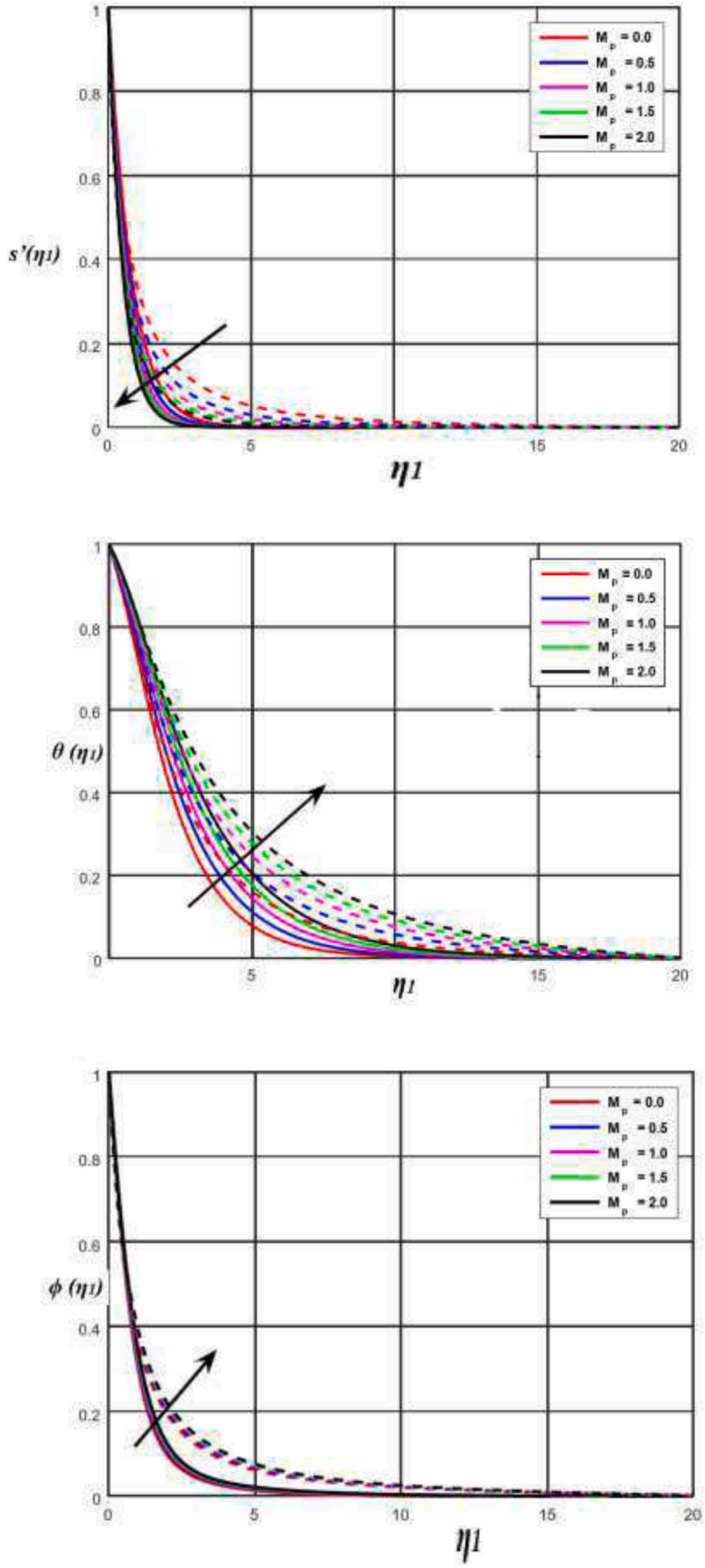


**Fig. 2.** Impact of *Mp* on velocity, temperature and concentration profiles.

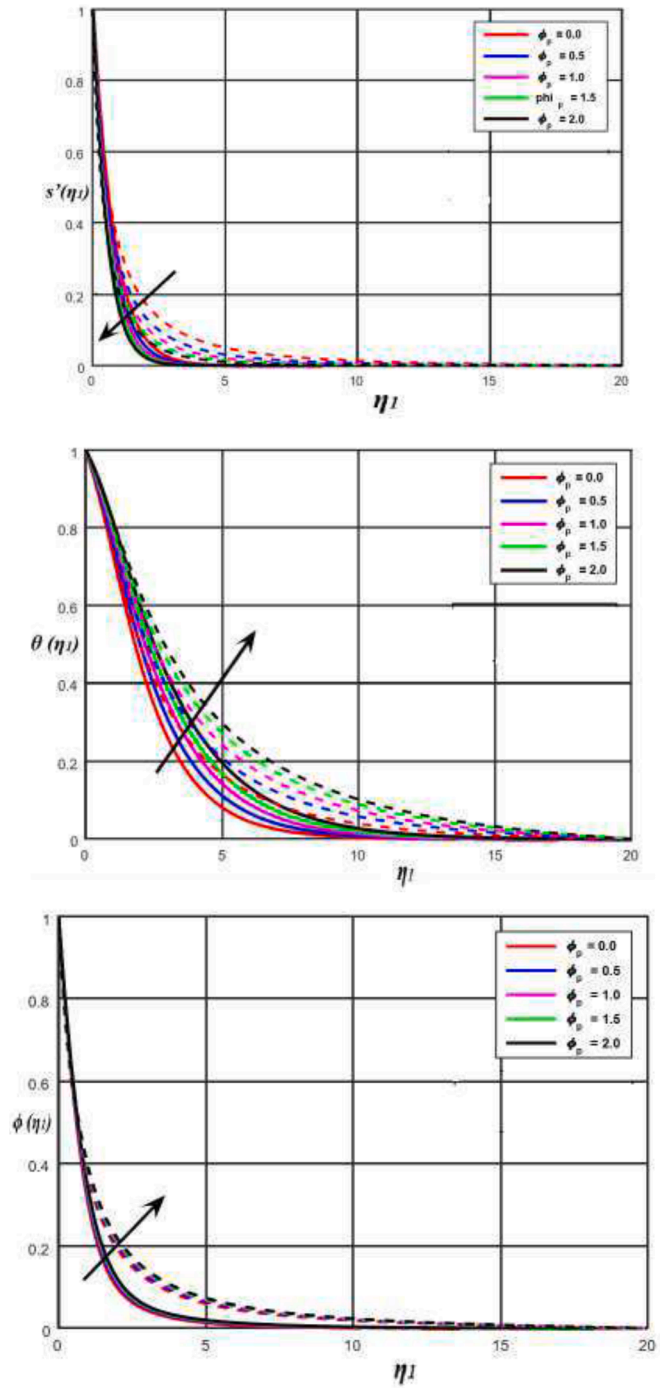


**Fig. 3.** Impact of porosity parameter on velocity, temperature and concentration profile.

### 3.4. Dimensionless energy equation

$$\left[(1+R_p)(1+2\eta_1\alpha)\right]\theta'' + 2(1+R_p)\alpha\,\theta' + Prs\,\theta' + Pr\,Q_p\theta = 0 \tag{8}$$

### 3.5. Dimensionless concentration equation

$$(1+2\eta_1\alpha)\phi'' + 2\alpha\phi' + Sc\,s\phi' = 0 \tag{9}$$

### 3.6. Dimensionless boundary condition

$$\begin{gathered} s(0) = \frac{Sb_m}{Sc}(1+2\eta_1\alpha)\phi'(0),\ \ s'(0) = 1,\ \ \theta(0) = 1,\ \ \phi(0) = 1 \\ s'(\infty) = 0,\ \ \theta(\infty) = 0,\ \ \phi(\infty) = 0 \end{gathered} \tag{10}$$

### 3.7. Skin friction coefficient

$$C_f = \frac{\tau_w}{\rho u_d^{*2}} = \mathrm{Re}_x^{\frac{-1}{2}}\, s''(0) \tag{11}$$

### 3.8. Nusselt number

$$Nu_x = \frac{z q_w}{k(T_w - T_\infty)},\ \ q_w = -k\frac{\partial T}{\partial r}\Big| r = h\ ,\quad Nu_x \mathrm{Re}_x^{\frac{-1}{2}} = -\theta'(0) \tag{12}$$

### 3.9. Sherwood number

$$Sh_x = \frac{z j_x}{D_B(C_w - C_\infty)},\ \ j_x = -D_B\frac{\partial C}{\partial r}\Big| r = h\ ,\quad Sh_x \mathrm{Re}_x^{\frac{-1}{2}} = -\phi'(0) \tag{13}$$

## 4. Solution method

The MATLAB function 'bvp4c' is designed for solving boundary value problems for ODEs. It is particularly useful when the boundary conditions are specified at more than one point. 'bvp4c' uses a collocation method to approximate the solution, making it suitable for both linear and nonlinear problems. Converting a nonlinear PDE into a linear form simplifies the problem, as linear equations are generally easier to solve analytically or numerically. Linearization often allows the use of established solution methods, ensures stability in numerical approaches, and makes the behavior of the system more predictable, hence the preference for linear forms in many practical scenarios.

$$s = O_1, s' = O_1' = O_2, s'' = O_2' = O_3, s''' = O_3',$$

$$\phi = O_6, \phi' = O_6' = O_7, \phi'' = O_7'$$

$$\theta = O_4, \theta' = O_4' = O_5, \theta'' = O_5',$$

The simplified governing equations can be expressed as

$$O_3' = \left[\frac{-2\alpha\, O_3 + O_2^2 - O_1\, O_3 - 2\beta_p O_1 O_2 O_3 + \frac{\alpha\beta_p}{(1+2\eta_1\alpha)} O_1^2 O_3 + M_p[O_2 - \beta_p O_1 O_3] + \phi_p O_2}{\left((1+2\eta_1\alpha) - \beta_p O_1^2\right)}\right] \tag{14}$$

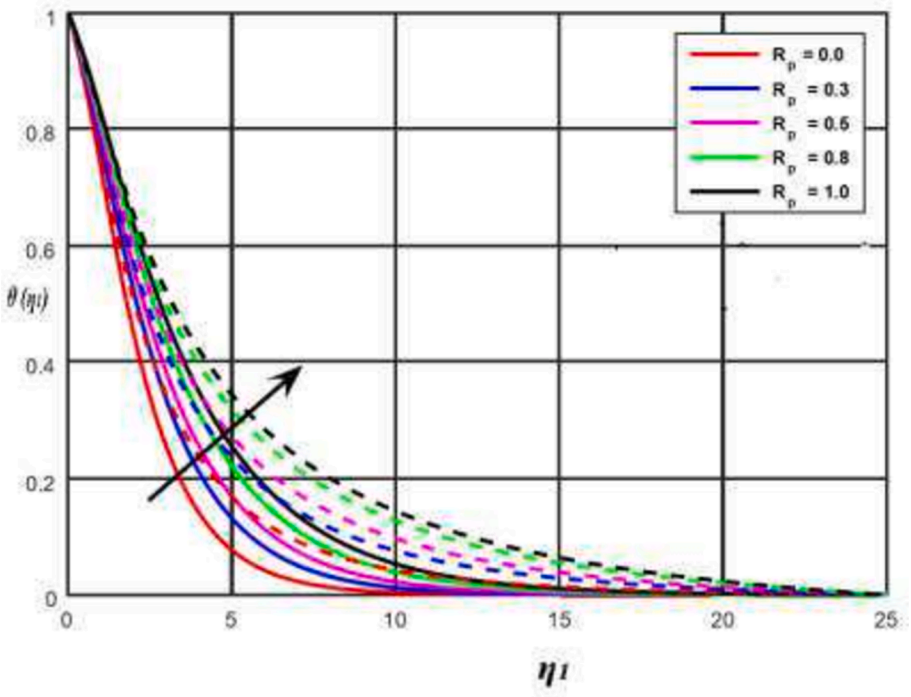


**Fig. 4.** Impact of radiation parameter on temperature profile, here solid line is for flat plates, curvature parameter $\alpha_e = 0$ and the dashed line is for cylindrical surfaces $\alpha_e = 1$.

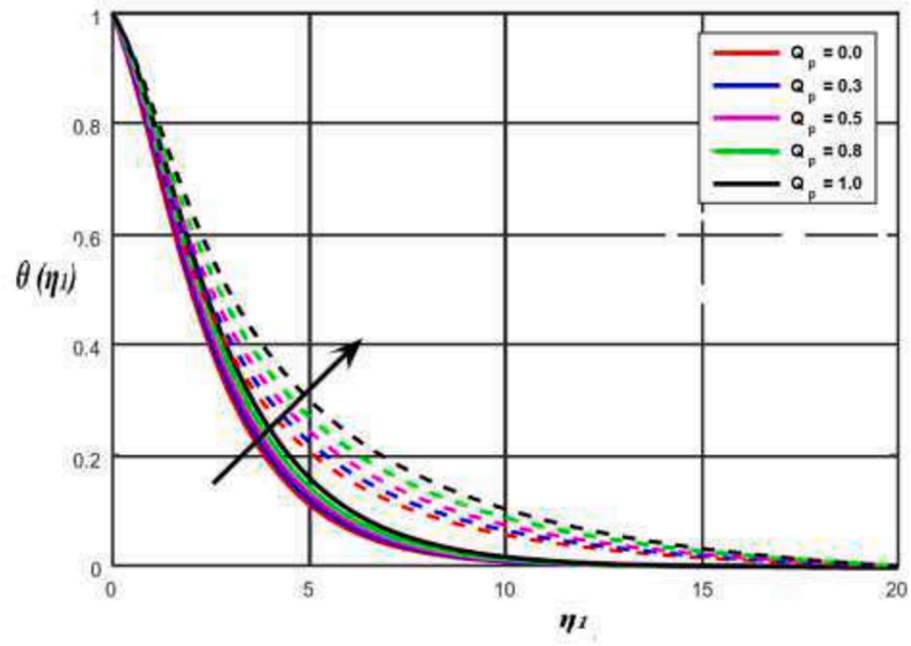


**Fig. 5.** Impact of heat generation parameter on temperature profile, here solid line is for flat plates, curvature parameter $\alpha_e = 0$ and the dashed line is for cylindrical surfaces $\alpha_e = 1$.

$$O_5^{'} = \frac{\left(-2(1+R_p)\alpha O_5 - PrO_1 O_5 - Pr\, Q_p O_4\right)}{\left[\left[(1+R_p)(1+2\eta_1\alpha)\right]\right]} \tag{15}$$

$$O_7^{'} = \frac{\left(-2\alpha O_7 - Sc\, O_1 O_7\right)}{\left[(1+2\eta_1\alpha)\right]} \tag{16}$$

## 5. Validation

A significant correlation was identified when the data were verified by comparison with publicly accessible information, as demonstrated in Table. 1. Table 2 displays the numerical data for the $Nu_x$ for distinct Pr values when chemical reaction and Brownian motions are zero in previous work of [24], our current work got good agreement. Table. 3 reveals that the skin friction profile increases with higher values of the MHD parameter, curvature parameter, and porosity parameter, while it

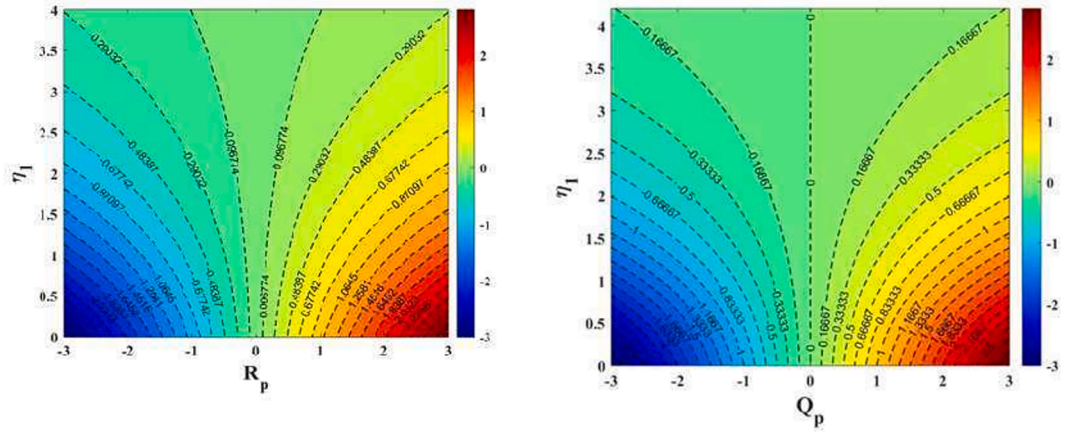


**Fig. 6.** Impact of radiation parameter $R_p = 2$ and heat generation parameter $Q_p = 0.5$ on Isotherm contour.

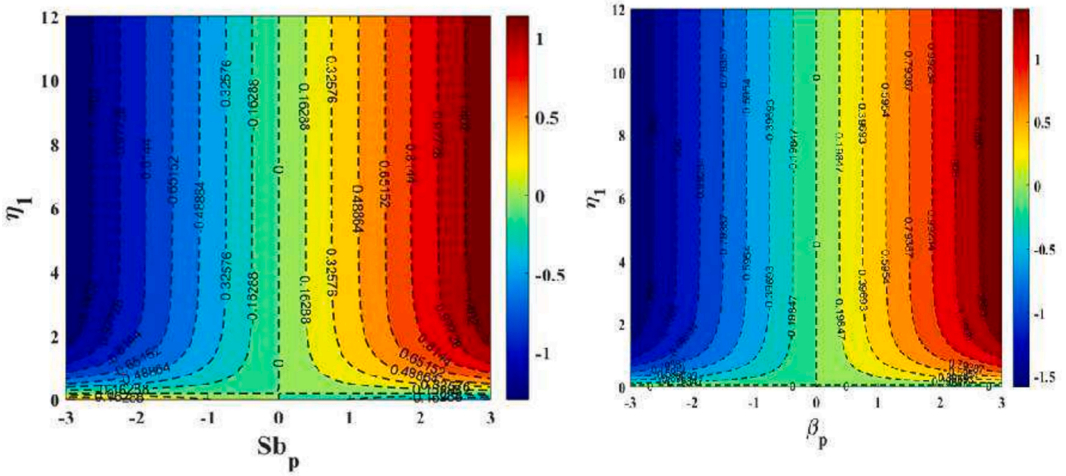


**Fig. 7.** Impact of Stefen parameter $Sb_p = 0.4$ and Maxwell fluid parameter $\beta_p = 0.4$ on streamline contour.

shows a slight increase with the radiation parameter. The Nusselt number profile decreases with increasing values of the MHD parameter, curvature parameter, and porosity parameter, but increases with the radiation parameter. In contrast, the Sherwood number profile decreases as the MHD parameter and porosity parameter increase, while it increases with the curvature parameter and remains almost unchanged with variations in the radiation parameter.

## 6. Results and discussions

Fig. 2 demonstrates the influence of the ($M_p$) magnetohydrodynamic parameter on the velocity, temperature, and concentration outlines. As the $M_p$ increases, the profile demonstrates a declining trend. This behavior can be attributed to the presence of a magnetic field, which exerts a Lorentz force that opposes the flow of the fluid, thereby reducing the fluid's velocity. The magnetic field effectively acts as a resistive force, slowing down the movement of charged particles in the fluid, leading to a reduction in the velocity outline. Conversely, the temperature outline exhibits an increasing trend with the rise in the $M_p$. The magnetic field's influence on the charged particles within the fluid causes an increase in Joule heating, which is the dissipation of electrical energy into heat.

Fig. 3 depicts the impact of the porosity parameter ($\phi_p$) on the velocity, temperature, and concentration outlines. As the $\phi_p$ increases, the profile shows a declining trend. This behavior is due to the increased resistance to fluid flow in a permeable medium. The porous structure hinders the movement of the fluid, creating more frictional resistance, which slows down the velocity of the flow through the medium. The higher the $\phi_p$, the more pronounced this effect becomes, leading to a significant reduction in velocity. In contrast, the temperature outline rises with a surge in the $\phi_p$. The reduced fluid velocity means that the fluid has more time to absorb and retain heat as it moves through the porous medium. Similarly, the concentration outline also increases with higher values of the porosity parameter. The slower fluid movement allows for more time for mass diffusion processes to occur within the medium. The porous structure can also facilitate greater mixing and diffusion of species, contributing to a surge in the concentration outline. As the fluid flow slows, the diffusion of particles becomes more effective, leading to a higher concentration of species within the fluid. This highlights the intricate relationship between fluid dynamics, heat transfer, and mass transfer in porous media systems.

Fig. 4 illustrates the effect of the radiation parameter ($R_p$) on the temperature outline, showing an upward trend as the radiation parameter increases. This behavior can be explained by the enhanced radiative heat transfer within the fluid. As the radiation parameter rises, the fluid absorbs more thermal energy from radiative sources, leading to an surge in the overall temperature. The heightened radiation contributes to a thicker thermal boundary layer and greater heat retention, resulting in a more pronounced rise in the temperature profile.

Fig. 5 demonstrates the impact of the heat generation parameter $Q_p$ on the temperature outline, which shows a swelling trend as the heat generation parameter rises. This effect occurs because the internal heat

generation within the fluid adds thermal energy, thereby raising the overall temperature. As the $Q_p$ increases, more heat is produced within the fluid, leading to a thicker thermal boundary layer and an elevated temperature profile. The additional heat generated enhances the fluid's capacity to retain thermal energy, resulting in the observed increase in temperature. This demonstrates the crucial role of internal heat generation in shaping the thermal behavior of the fluid.

Fig. 6 shows the impact of $R_p = 2$ and the heat generation parameter $Q_p = 0.5$ on the isotherm contours. The isotherm contours exhibit a significant rise in temperature due to the combined effects of $R_p$ and internal $Q_p$. The radiation parameter enhances radiative heat transfer within the fluid, increasing the thermal energy absorbed and retained by the fluid. Simultaneously, the heat generation parameter contributes additional thermal energy from within the fluid, further elevating the temperature.

Fig. 7 illustrates the impact of the Stefan parameter $Sb_p = 0.4$ and the Maxwell fluid parameter $\beta_p = 0.4$ on the streamline contours. The streamline patterns show noticeable changes due to the combined influence of these parameters. The Stefan parameter, associated with phase change phenomena, affects the fluid's flow characteristics by altering the energy transfer and energy distribution within the system. Concurrently, the $\beta_p$, which characterizes the viscoelastic nature of the fluid, influences the fluid's deformation and flow behavior. Together, these parameters create a more complex flow pattern, reflected in the streamlined contours. The viscoelastic nature of the Maxwell fluid, combined with the heat transfer effects driven by the Stefan parameter, leads to a more intricate and modified flow structure within the fluid.

## 7. Conclusions

The primary aim of this manuscript was to examine the thermal and flow behavior of Maxwell fluids under the impact of magnetohydrodynamics, $R_p$, and $Q_p$ over a stretching cylinder. The study specifically focused on understanding how the curvature parameter impacts these dynamics, with the results providing significant insights relevant to industrial applications such as polymer processing and heat exchangers. The governing equations were derived, shortened using similarity transformations, and solved numerically using bvp4c solver. The key findings are summarized here.

- Increasing the magnetic parameter reduces velocity due to the Lorentz force, while temperature and concentration profiles rise from enhanced Joule heating and diffusion.
- Higher porosity decreases velocity due to added resistance, but temperature and concentration increase, indicating extended heat retention and diffusion.
- Radiation parameter increases the temperature profile, enhancing heat transfer and thickening the thermal boundary layer.
- Similarly, higher heat generation elevates temperature due to internal heat production, thickening the boundary layer.
- Combined effects of radiation and heat generation significantly raise temperature contours.
- Stefan and Maxwell parameters create a complex flow pattern, influenced by phase change and viscoelastic effects.
- This study provides insights into the combined impact of these parameters on Maxwell fluid flow, aiding in process optimization.

## 8. Future work

Future work could include studying non-Newtonian fluids with variable properties under MHD, radiation, and heat generation. Exploring time-dependent boundary conditions, transient heat transfer, and multi-phase flow dynamics would offer deeper insights. Three-dimensional analysis and experimental validation would further improve the accuracy and applicability of the findings for industrial processes.

**Institutional Review Board Statement:** Not applicable.
**Informed Consent Statement:** Not applicable.

## CRediT authorship contribution statement

**Umadevi Raj:** Writing – original draft, Project administration, Formal analysis, Data curation. **Prabhakar Sagadevan:** Writing – review & editing, Resources, Investigation. **Nazek Alessa:** Project administration, Methodology, Funding acquisition.

## Declaration of competing interest

The authors declare that they have no known competing financial interests or personal relationships that could have appeared to influence the work reported in this paper.

## Acknowledgements

Princess Nourah Bint Abdulrahman University Researchers Supporting Project number (PNURSP2024R59), Princess Nourah Bint Abdulrahman University, Riyadh, Saudi Arabia

## Appendix A. Supplementary data

Supplementary data to this article can be found online at https://doi.org/10.1016/j.jksus.2024.103530.

## References

Ahmed, A., Khan, M., Irfan, M., Ahmed, J., 2020 Dec. Transient MHD flow of Maxwell nanofluid subject to non-linear thermal Radiation and convective heat transport. Appl. Nanosci. 10, 5361–5373. https://doi.org/10.1007/s13204-020-01375-1.

Biswas, N., Mondal, M.K., Mandal, D.K., Manna, N.K., Gorla, R.S., Chamkha, A.J., 2022 Mar. A narrative loom of hybrid nanofluid-filled wavy walled tilted porous enclosure imposing a partially active magnetic field. Int. J. Mech. Sci. 1 (217), 107028.

Biswas, N., Chatterjee, D., Sarkar, S., Manna, N.K., 2024 Feb 23. Magneto-nanofluidic thermal transport and irreversibility in semicircular systems with heated wavy bottom under constant fluid volume and cooling surface constraints. Int. J. Numer. Meth. Heat Fluid Flow 34 (2), 1021–1059.

Crane, L.J., 1975 Sep. Boundary layer flow due to a stretching cylinder. Zeitschrift Für Angewandte Mathematik Und Physik ZAMP. 26 (5), 619–622.

Grubka, L.J., Bobba, K.M., 1985 Feb 1. Heat transfer characteristics of a continuous stretching surface with variable temperature. J. Heat Transfer 107 (1), 248–250.

Irfan, M., Khan, M., Khan, W.A., Ayaz, M., 2018 Aug 2. Modern development on the features of magnetic field and heat sink/source in Maxwell nanofluid subject to convective heat transport. Phys. Lett. A 382 (30), 1992–2002. https://doi.org/10.1016/j.physleta.2018.05.008.

Ishak, A., 2010 Jun. Thermal boundary layer flow over a stretching sheet in a micropolar fluid with radiation effect. Meccanica 45, 367–373. https://doi.org/10.1007/s11012-009-9257-4.

Khan, M., Ahmed, A., Irfan, M., Ahmed, J., 2021 Apr. Analysis of Cattaneo–Christov theory for unsteady flow of Maxwell fluid over stretching cylinder. J. Therm. Anal. Calorim. 144, 145–154.

Loganathan, K., Alessa, N., Namgyel, N., Karthik, T.S., 2021 Jun. MHD flow of thermally radiative Maxwell fluid past a heated stretching sheet with Cattaneo–Christov dual diffusion. J. Math. (Wuhan) 22 (2021), 1.

Mandal, D.K., Biswas, N., Manna, N.K., Gorla, R.S., Chamkha, A.J., 2022 Sep. Magneto-hydrothermal performance of hybrid nanofluid flow through a non-Darcian porous complex wavy enclosure. The European Physical Journal Special Topics. 231 (13), 2695–2712.

Mandal, D.K., Biswas, N., Manna, N.K., Gorla, R.S., Chamkha, A.J., 2023 Jan 5. Hybrid nanofluid magnetohydrodynamic mixed convection in a novel W-shaped porous system. Int. J. Numer. Meth. Heat Fluid Flow 33 (2), 510–544.

Manna, N.K., Saha, A., Biswas, N., Ghosh, K., 2024 Apr 3. Constraint-based analysis of heat transport and irreversibility in magnetic nanofluidic thermal systems. Int. J. Numer. Meth. Heat Fluid Flow.

Mukhopadhyay, S., 2012 May 1. Heat transfer analysis of the unsteady flow of a Maxwell fluid over a stretching surface in the presence of a heat source/sink. Chin. Phys. Lett. 29 (5), 054703.

Ramzan, M., Bilal, M., Chung, J.D., Farooq, U., 2016 Jan. Mixed convective flow of Maxwell nanofluid past a porous vertical stretched surface–An optimal solution. Results Phys. 1 (6), 1072–1079. https://doi.org/10.1016/j.rinp.2016.11.036.

Reddy Gorla, R.S., Sidawi, I., 1994 Apr. Free convection on a vertical stretching surface with suction and blowing. Appl. Sci. Res. 52, 247–257.

Wang, C.Y., 1988 Mar. Fluid flow due to a stretching cylinder. The Physics of Fluids. 31 (3), 466–468.
Yang, X., Lu, T., Kim, T., 2013 Jan 1. Thermal stretching in two-phase porous media: Physical basis for Maxwell model. Theor. Appl. Mech. Lett. 3 (2), 021011. https://doi.org/10.1063/2.1302111.
Zhao, J., 2020 Oct. Axisymmetric convection flow of fractional Maxwell fluid past a vertical cylinder with velocity slip and temperature jump. Chin. J. Phys. 1 (67), 501–511.

## Further reading

Ahmed, A., Alhowaity, S., Ghoneim, M.E., Gamaoun, F., Tag-eldin, E., Yassen, M.F., Sarfraz, M., 2022. Material and wave relaxation phenomena effects on the rheology of Maxwell nanofluids. Frontiers. Physics 886, 1005056. https://doi.org/10.3389/fphy.2022.1005056.
Al Nuwairan, M., Hafeez, A., Khalid, A., Souayeh, B., Alfadhli, N., Alnaghmosh, A., 2022 Oct 17. Flow of Maxwell Fluid with Heat Transfer through Porous Medium with Thermophoresis Particle Deposition and Soret–Dufour Effects: Numerical Solution. Coatings 12 (10), 1567.
Irfan, M., Khan, M., Khan, W.A., 2019 Mar. Impact of homogeneous–heterogeneous reactions and non-Fourier heat flux theory in Oldroyd-B fluid with variable conductivity. J. Braz. Soc. Mech. Sci. Eng. 41, 1–9. https://doi.org/10.1007/s40430-019-1619-9.
Maxwell, J.C., 1881. A treatise on electricity and magnetism: Pt. Clarendon press, III. Magnetism. pt. IV. Electromagnetism.
Merkin, J.H., Najib, N., Bachok, N., Ishak, A., Pop, I., 2017 May. Stagnation-point flow and heat transfer over an exponentially stretching/shrinking cylinder. J. Taiwan Inst. Chem. Eng. 1 (74), 65–72.
Sajjad Saif, R., Haneef, M., Nawaz, M., Muhammad, T., 2023. Transport mechanism under temperature and concentration gradient for nano-sized species in Maxwell viscoelastic fluid over cylindrical object moving with non-uniform velocity. Chem. Phys. Lett. 813, 140293.
Shah, S., Rafiq, N., Abdullah, F.A., Atif, S.M., Abbas, M., 2022 Feb. Slip and radiative effects on MHD Maxwell nanofluid with non-Fourier and non-Fick laws in a porous medium. Case Stud. Therm. Eng. 1 (30), 101779.
Subbarao K, Elangovan K, Gangadhar K. Slippery boundary and radiative transport in unsteady features of Maxwell fluid over stretched cylinder. Journal of Taibah University for Science. 2023; 17(1).
Sudarmozhi, K., Iranian, D., Khan, I., 2023 Jun. Heat and mass transport of MHD viscoelastic fluid flow towards a permeable stretching cylinder. Int. Commun. Heat Mass Transfer 1 (145), 106864.
Wang, C.Y., Ng, C.O., 2011 Nov 1. Slip flow due to a stretching cylinder. Int. J. Non Linear Mech. 46 (9), 1191–1194.